



Open Archive Toulouse Archive Ouverte (OATAO)

OATAO is an open access repository that collects the work of some Toulouse researchers and makes it freely available over the web where possible.

This is an author's version published in: <http://oatao.univ-toulouse.fr/21651>

Official URL: <https://doi.org/10.1080/15376494.2018.1519619>

To cite this version:

Susainathan, John and Eyma, Florent and De Luycker, Emmanuel and Cantarel, Arthur and Castanié, Bruno Numerical modeling of impact on wood-based sandwich structures. (2019) Mechanics of Advanced Materials and Structures. ISSN 1537-6494

Any correspondence concerning this service should be sent to the repository administrator:

tech-oatao@listes-diff.inp-toulouse.fr

Numerical modeling of impact on wood-based sandwich structures

John Susainathan^a, Florent Eyma^a, Emmanuel DE Luycker^{a,b}, Arthur Cantarel^a, and Bruno Castanie^a

^aCNRS UMR 5312-INSA-ISAE-Mines Albi-UPS, Institut Clément Ader (ICA), Université de Toulouse, Toulouse, France; ^bEA 1905 INP-ENIT, Laboratoire Génie de Production (LGP), Université de Toulouse, Tarbes, France

ABSTRACT

The impact behavior of innovative wood based sandwich structures with plywood core and skins made either of aluminum or of fiber reinforced polymer (carbon, glass, or flax composite skins) was investigated numerically. The wood based sandwich structures were subjected to low-velocity/low-energy impacts. An explicit nonlinear numerical model based on volume elements with a cohesive layer was developed. A plastic wood law already implemented in LS-DYNA was used in association with composite type damage criteria. Comparisons with experiments in terms of layer deformations and overall contact laws during impact showed satisfactory results.

KEYWORDS

Wood; impact; sandwich; damage; finite element model

1. Introduction

Sandwich structures are well known, efficient structures that are widely used in numerous sectors such as the automotive, aerospace, marine and energy industries, due to their high specific bending strength and stiffness, excellent damping and thermal insulation. Their main drawback is their naturally complex mechanical behavior, such as local buckling, which leads to cautious designs with large safety margins [1]. Another drawback is their cost and the authors have already presented a low cost sandwich structure based on a plywood core and stiffer skins made of aluminum alloy or composite [2]. The development of such structures requires many investigations before their dissemination. After a first static analysis [2], the authors focused on the issue of low-velocity/low-energy impact, which is a major concern for the sizing of sandwich structures [3–5]. The main results of the experimental part of that study are shown in reference [6] and thus the aim of the present paper is to model impact for those particular sandwich structures.

Many modeling strategies have been developed to model impacts on sandwich structures. Among others, Aminanda et al. [7, 8] have developed a discrete model of honeycomb core which is based on the understanding of postbuckling behavior during crushing of Nomex. It allows indentation, low velocity impact, residual dent and compression after impact strength to be finely captured for sandwiches with metallic skins. Different strategies must be used for other cores, such as foams, mainly using Continuum Damage Mechanics and ad-hoc laws to capture the nonlinear behavior [9–13]. More complex behaviors of skins are involved in the case of composite skins and very advanced models can now capture the discrete nature of the failure scenarios [14–19]. However, these models remain very complex and

require in-house finite elements or software. In our case, a robust strategy, available in commercial software, is required to model damage in the skins and in the plywood core. For the skins, it is now common to use PFA (Progressive Failure Analysis) and the results are often acceptable [20–24]. For the plywood core, a specific approach must be chosen.

Many authors have studied the behavior of wood but rarely under dynamic loading [25]. Polocoşer et al. made a comprehensive review of dynamic testing on solid wood [26]. They argue that, due to the complexity of wood behavior, including viscoelastic effects, progress still needs to be made to enhance tests and to interpret the results finely.

The most common wood studied in sandwich composites under impact is balsa but it is mostly investigated from an experimental point of view or for comparison purposes, for example [27–29]. However, several authors have focused more precisely on the modeling of the crushing of wood. Toson et al. [30] studied balsa used as an energy absorber and developed a model taking account of the principal phenomena observed experimentally. The complex nonlinear properties of wood, such as non-isotropy, non-linear compressibility, softening, densification, and rate-dependency, were considered for the states of compression and shear over a large range of strain rates. Vural and Ravichandran [31] studied the dynamic behavior of balsa with Hopkinson's bars, analyzing and modeling compression and kink band formation in the cell walls. However, these models are better suited to large strain rates, which are not reached in low-velocity/low-energy impacts. Thus, a comprehensive model describing the behavior of wood, and already implemented in LS-DYNA code by Murray, is used in our context [32, 33].

The experimental results presented in [6] support the modeling strategy presented in this research. A 10 mm plywood core was considered in order to be able to compare

Table 1. Manufactured specimens.

Core	Skin	Process	Relative density	Total Thickness (mm)	Process specification
Plywood A	–	–	0.461	10	–
Plywood B	–	–	0.433	10	–
Plywood A	Aluminum	–	0.678	11	–
Plywood A	Glass	Vacuum bag molding - Prepreg	0.638	12	At 160 °C for 3 h
	Carbon		0.569		
Plywood B	Flax	Thermo-compression - Prepreg	0.488	12	At 120 °C with pressure of 4 bar for 1 h
	Carbon		0.614		
	Glass		0.609		At 90 °C for 30 min then at 125 °C for 1 h At 160 °C with pressure of 4 bar for 3 h

Table 2. Plywood A and B stacking.

Type	Ply	Orientation	Thickness (mm)
Plywood - A	Okoume	0°	1
	Okoume	90°	1
	Poplar	0°	2
	Poplar	90°	2
	Poplar	0°	2
	Okoume	90°	1
Plywood - B	Okoume	0°	1
	Poplar	90°	3
	Okoume	0°	2
	Poplar	90°	3
	Okoume	0°	1
	Okoume	0°	1

the effects of skins made of aluminum alloy, and composites reinforced with glass, carbon fibers or flax, on their impact behavior (see [2] for manufacturing details and issues). These materials were impacted at energies of 5 J, 10 J, and 15 J using a drop-weight impact test. A comparison based on the force–displacement response and failure modes of the panels will be recalled briefly in the following subsection, together with additional results. Damage resistance and failure modes of wood based sandwich structures under low energy impact will be described using post impact tomography analysis. Numerical modeling of the impact response of these panels will be performed using the finite element software LS-DYNA to correlate experimental results.

2. Experimental investigations

2.1. Specimens and tests

Two different plywoods and six different configurations of wood based sandwich structures were used and manufactured as noted in Table 1 (for more detailed information see [2, 6, 33]). The stacking patterns of the plywood are shown in Table 2. Skins were made of aluminum or a composite of polymer reinforced with fibers of carbon, glass or flax. Large plates of dimensions $500 \times 500 \text{ mm}^2$ were manufactured and then cut into $150 \times 100 \text{ mm}^2$ samples for impact testing so as to follow AIRBUS standard AITM 1-0010. For each material configuration, three tests were performed: at 5 J, 10 J and 15 J (one specimen per configuration and energy level). Impact tests were performed using a drop weight apparatus (Figure 1), the same device as used in [34], followed by tomography analysis. The main characteristics of our test are recalled below:

- A mass of about 2.08 kg. This mass value was set so as to achieve high enough impact energy with speeds of up to 5 m/s.

- A load sensor located under the mass, which measured the force between the impactor and the specimen during the impact;
- A 16 mm diameter hemispherical impactor;
- An optical sensor that measured the speed of the impactor immediately before impact
- A support window, of internal dimensions $125 \times 75 \text{ mm}^2$, on which the specimen was laid (standard specimen dimensions: $100 \times 150 \text{ mm}^2$ based on Airbus standards AITM 1-0010).
- A clamping window with inner dimensions identical to those of the lower window ($125 \times 75 \text{ mm}^2$) to hold the specimen during impact.
- A kickback system to prevent multiple shocks to the specimen;

Low velocity impact tests were carried out at various impact energies: 5 J, 10 J and 15 J. These energy levels correspond to impacts due to the dropping of tools, for example. The orientation of the top plies of the sample served as a reference for the longitudinal and transverse directions. Typical experimental force-displacement curves are shown Figure 2 for an impact at 10 J (see [6] and [33] for more details).

2.2. Additional experimental results

A typical post-impact pattern is presented in Figure 3. It can be seen that each ply undergoes severe transverse compression. It is pertinent to analyze the behavior of the plywood using the deformation of each ply. This analysis will be useful for numerical comparisons. The thickness after impact and the percentage of thickness decrease between the pristine state and after impact are provide in Tables 3–10 for the eight configurations tested.

3. Numerical model description

3.1. Overall model description

This section presents the numerical simulation of the impact tests carried out in LS-DYNA. Eight-node solid finite elements with one integration point were used. A quarter symmetric model was considered as shown in Figure 4. The support and impactor were taken to be rigid (i.e. undeformable). The impactor was modeled with 1,952 solid elements. An initial velocity V_{imp} was imposed on the impactor, as measured during experiments, and the impactor mass was chosen in order to respect its experimental kinetic energy. In the case of plywood structures, twenty elements were



Figure 1. Drop-weight impact test set-up and aluminum wood specimen installed.

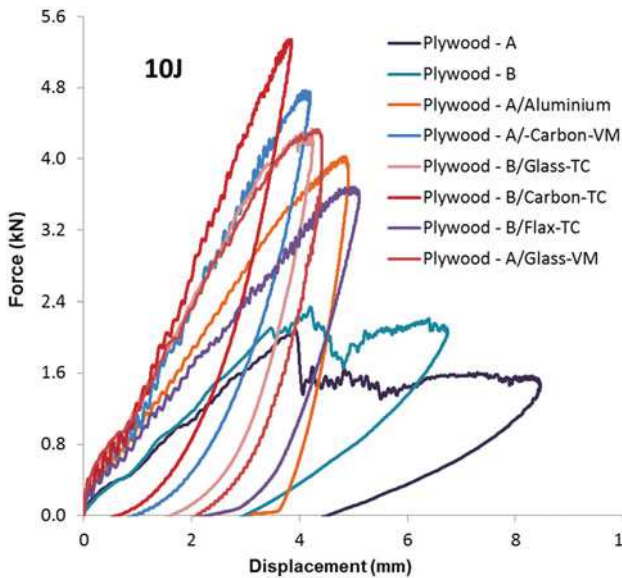


Figure 2. Typical load displacement curves for 10 J impacts for the eight configurations tested.

meshed in their total thickness, which means 2 elements per mm in the thickness. So, in the case of the plywood core sandwich, total plywood core A or B was meshed with 33,920 elements (Figure 4). The transverse isotropic wood material model (MAT_143) available in LS-DYNA was used to model each ply of the plywood core. A local in-plane mesh refinement was used in the impact region, as shown in Figure 4, to obtain precise strain and stress gradients. The sandwich structures with plywood core and aluminum skin were composed of one layer of aluminum for the top and bottom skins and a plywood core A, having four okoume plies and three poplar plies with different fiber orientations as shown in Figure 5. The mesh geometry of the 0.5 mm thick skins was designed with two elements in the thickness. Each skin was modeled with 3,392 elements. For plywood structures with composite skins, such as carbon, glass, and flax, the same impact model as shown in Figure 4 was used. The same mesh geometry for plywood A or B core led to the same number of elements (33,920 elements). The top and bottom composite skins were modeled with six elements in the thickness, so 10,176 elements were used for each composite skin. A layer of four nodes with zero thickness cohesive elements was inserted between the plies of

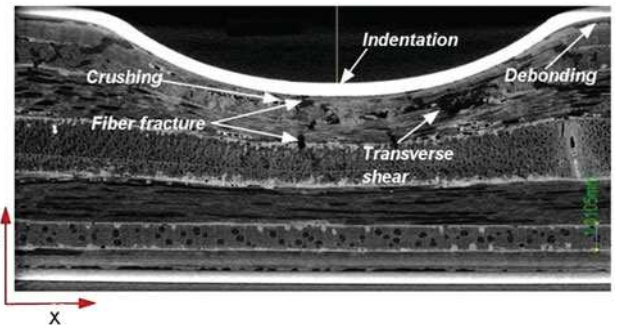


Figure 3. Tomography images of the center of impacted plywood with aluminum skin – Failure pattern at 15 J.

different fiber orientation composing the skins and also between the skins and the core as shown in red in Figure 5.

For all types of plywood sandwich with different skins, Tied_Nodes_To_Surface offset was utilized in the plywood core between plies of different fiber orientation. A layer of 4 point cohesive elements was used between the skins and the core as illustrated in Figure 5. These cohesive elements share nodes with the solid elements. When failure occurs, the cohesive elements are deleted from the simulation. To avoid errors due to negative element volume, a type 5 hourglass control and energy (HGE) coefficient value of 0.03 was used in the plywood core. An automatic_surface_to_surface contact, suitable for low energy/low velocity impact, was defined between the impactor and the top ply of the core and also at the interface between plies of plywood core in order to implement non-erosion.

Eroding single surface contact is strongly preferred between solid and cohesive elements, which can enable the model to establish contact between the surfaces through deletion of cohesive elements upon failure [35]. Hence, Eroding_Single_Surface contact was used between the cohesive layers and the skins and also between the core and the cohesive layers. An Automatic_surface_to_surface contact was defined between plies, which became active when a cohesive element was deleted using eroding contact. The same contact type was also used between the skin and the impactor.

3.2. Material laws used and identification of mechanical characteristics for plywoods and skins

The elastic and other material characteristics of each ply of the plywood core and of the skins were found semi-empirically by

Table 3. Ply thickness analysis after impact for Plywood A.

Plywood - A	Orientation	Reference thickness (mm)	Thickness (mm)			Thickness drop (%)		
			5 J	10 J	15 J	5 J	10 J	15 J
Okoume	0	0.69	0.42	0.33		40	52	
Okoume	90	0.94	0.72	0.70		23	26	
Poplar	0	1.94	1.07	0.99		45	49	
Poplar	90	2.05	1.55	1.34		24	35	
Poplar	0	1.91	1.91	1.73		0	10	
Okoume	90	0.89	0.89	0.89		0	0	
Okoume	0	0.66	0.66	0.66		0	0	

Table 4. Ply thickness analysis after impact for Plywood B.

Plywood - B	Orientation	Reference thickness (mm)	Thickness			Thickness drop (%)		
			5 J	10 J	15 J	5 J	10 J	15 J
Okoume	0	0.97	0.42	0.67		57	31	
Poplar	90	2.89	1.80	1.47		38	49	
Okoume	90	1.84	1.67	1.56		9	15	
Poplar	90	2.94	2.94	2.84		0	3	
Okoume	0	0.95	0.95	0.94		0	1	

Table 5. Ply thickness analysis after impact for Plywood A with aluminum skins.

Plywood - A/Al	Orientation	Reference thickness (mm)	Thickness (mm)			Thickness drop (%)		
			5 J	10 J	15 J	5 J	10 J	15 J
Al		0.5	0.49	0.47	0.47	3	6	6
Okoume	0	0.69	0.40	0.47	0.45	41	32	35
Okoume	90	0.94	0.38	0.34	0.32	59	64	66
Poplar	0	1.94	0.71	0.67	0.62	64	65	68
Poplar	90	2.05	1.80	1.53	1.52	12	25	26
Poplar	0	1.91	1.91	1.91	1.70	0	0	11
Okoume	90	0.89	0.89	0.89	0.89	0	0	0
Okoume	0	0.66	0.66	0.66	0.66	0	0	0
Al		0.5	0.50	0.50	0.50	0	0	0

Table 6. Ply thickness analysis after impact for Plywood A with carbon skins.

Plywood - A/Carbon	Orientation	Reference thickness (mm)	Thickness (mm)			Thickness drop (%)		
			5 J	10 J	15 J	5 J	10 J	15 J
Carbon		0.85	0.80	0.80	0.76	6	6	11
Okoume	0	0.53	0.44	0.44	0.41	16	17	22
Okoume	90	0.95	0.84	0.80	0.79	11	15	17
Poplar	0	1.94	1.75	1.69	1.65	10	13	15
Poplar	90	2.00	1.99	1.84	1.72	0	8	14
Poplar	0	1.99	1.99	1.99	1.99	0	0	0
Okoume	90	0.99	0.99	0.99	0.99	0	0	0
Okoume	0	0.58	0.58	0.58	0.58	0	0	0
Carbon		0.91	0.91	0.91	0.91	0	0	0

Table 7. Ply thickness analysis after impact for Plywood B with carbon skins.

Plywood - B/Carbon	Orientation	Reference thickness (mm)	Thickness			Thickness drop (%)		
			5J	10J	15J	5J	10J	15J
Carbon		0.78	0.77	0.76	0.76	1	3	3
Okoume	0	0.91	0.77	0.77	0.69	15	16	24
Poplar	90	2.89	2.67	2.65	2.24	8	8	23
Okoume	0	1.89	1.89	1.89	1.76	0	0	7
Poplar	90	2.94	2.94	2.94	2.94	0	0	0
Okoume	0	0.79	0.79	0.79	0.79	0	0	0
Carbon		0.78	0.78	0.78	0.78	0	0	0

Table 8. Ply thickness analysis after impact for Plywood A with glass skins.

Plywood - A/Glass	Orientation	Reference thickness (mm)	Thickness (mm)			Thickness drop (%)		
			5 J	10 J	15 J	5 J	10 J	15 J
Glass		0.99	0.99	0.99	0.98	0	0	1
Okoume	0	0.53	0.39	0.30	0.24	26	44	55
Okoume	90	0.99	0.84	0.81	0.67	16	18	33
Poplar	0	1.94	1.89	1.50	1.38	3	22	29
Poplar	90	2.00	2.00	1.92	1.69	0	4	15
Poplar	0	1.99	1.99	1.99	1.99	0	0	0
Okoume	90	0.99	0.99	0.99	0.99	0	0	0
Okoume	0	0.58	0.58	0.58	0.58	0	0	0
Glass		0.99	0.99	0.99	0.99	0	0	0

Table 9. Ply thickness analysis after impact for Plywood B with glass skins.

Plywood - B/Glass	Orientation	Reference thickness (mm)	Thickness (mm)			Thickness drop (%)		
			5 J	10 J	15 J	5 J	10 J	15 J
Glass		0.99	0.97	0.95	0.88	2	4	11
Okoume	0	0.97	0.97	0.88	0.88	0	9	9
Poplar	90	2.89	2.89	2.43	2.18	0	16	25
Okoume	0	1.87	1.87	1.84	1.74	0	2	7
Poplar	90	2.94	2.94	2.94	2.62	0	0	11
Okoume	0	0.95	0.95	0.95	0.95	0	0	0
Glass		0.99	0.99	0.99	0.99	0	0	0

Table 10. Ply thickness analysis after impact for Plywood B with flax skins.

Plywood - B/Flax	Orientation	Reference thickness (mm)	Thickness (mm)			Thickness drop (%)		
			5 J	10 J	15 J	5 J	10 J	15 J
Flax		0.78	0.75	0.74	0.72	5	6	8
Okoume	0	0.97	0.75	0.62	0.61	23	36	37
Poplar	90	2.89	2.02	1.87	1.57	30	36	46
Okoume	0	1.84	1.84	1.66	1.57	0	10	14
Poplar	90	2.94	2.94	2.94	2.94	0	0	0
Okoume	0	0.95	0.95	0.95	0.95	0	0	0
Flax		0.78	0.78	0.78	0.78	0	0	0

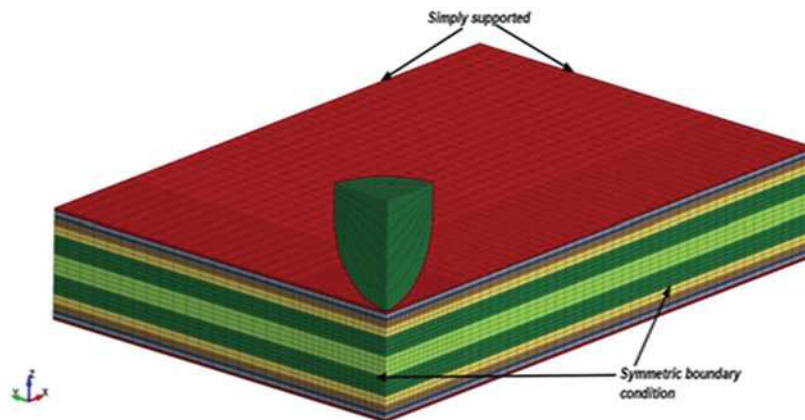


Figure 4. Numerical model for drop-weight impact.

reverse identification with the help of the three point bending tests carried out by the authors [2]. Individual identification of each linear and nonlinear characteristic would have been too long and complex and beyond the scope of the present study. The initial material constants for the numerical impact model were chosen from the literature, for example [36].

3.2.1. Damage laws for plywood core

The elastic and plastic properties of wood are different in the longitudinal, tangential, and radial directions. This is naturally represented by orthotropic behavior. At a macroscopic scale, wood can be considered as a continuous, homogenous material, especially when dealing with first grade plywood materials where knots and heterogeneities

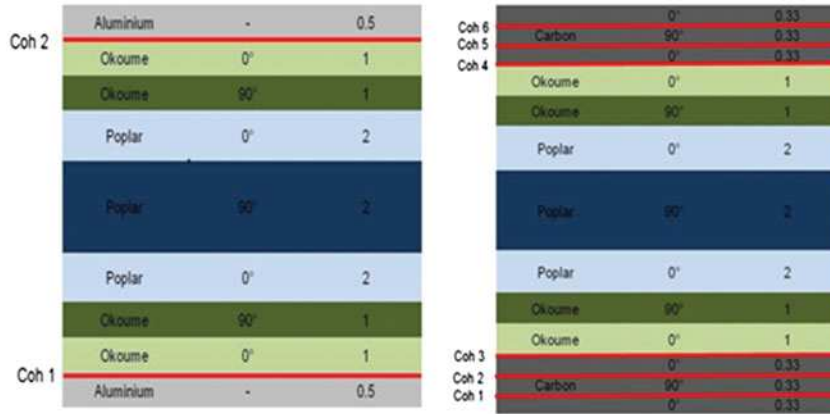


Figure 5. Cohesive element locations (red lines – color figure available online).

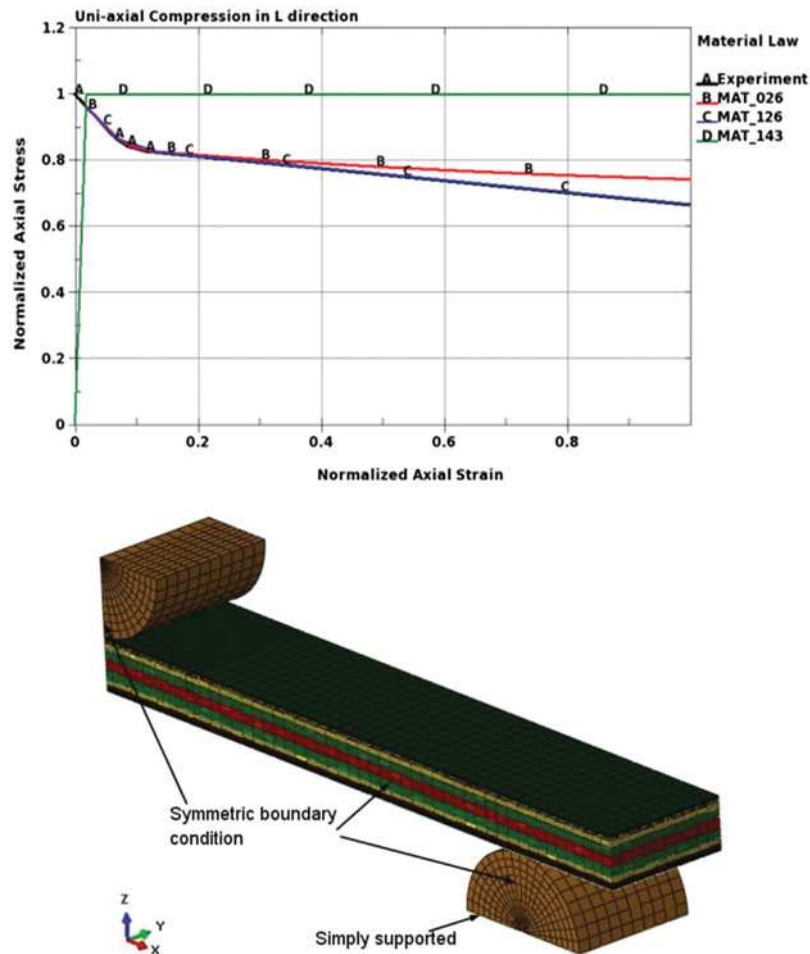


Figure 6. Uni-axial compressive numerical model [7]. Three point bending numerical model.

have been carefully removed. The longitudinal direction in wood is always much stiffer and stronger than the other two, which have comparable behavior. Hence, transverse isotropic material behavior can efficiently reproduce the main behavior of wood. Considering the compressive response of wood, four main stages can be distinguished [37]: first, an elastic part ended by a softening where the wood cell wall starts to collapse, then a plateau, where the crushing of wood cells continues, and, finally, a densification. At micro level, wood has a cellular structure similar to honeycomb [7]. Micro-

buckling of tracheid (cell walls) occurs during longitudinal compression and this mechanism can be compared to the macro-buckling of cell walls in metallic square tube structures [37] used for dissipating energy in a crash-box. Hence, Maillot et al. [38] compare three different material models in LS-DYNA, such as the honeycomb material model (MAT_26), the modified honeycomb material model (MAT_126) and the Wood material model (MAT_143), in order to improve the modeling of the longitudinal compression response of balsa wood. Maillot et al. found that the

current wood material model (MAT_143) could only tune the transition between an elastic and a plastic phase. It represents wood behavior as elastic-perfectly plastic and unable to include the softening behavior preceding the plateau in compression along the fiber direction (see Figure 6). Their comparative study leads to an improved and more representative wood material model able to represent softening behavior in FE models. For plywood structures, fiber fracture, debonding, crushing and transverse shear are identified as primary failure modes under low-velocity/low-energy impact [6]. In order to represent the above failure modes, each ply of the plywood core is modeled with the wood material model (MAT_143) in LS-DYNA. In this model, transverse isotropic behavior is considered with a modified Hashin failure criterion. In this criterion, compressive and shear stresses are assumed to be mutually weakening, so a compressive parallel and perpendicular criterion similar to that for tensile loading can be assumed. Damage evolution is computed through parallel and perpendicular mode fracture energy parameters, which are obtained from stress intensity factors in modes I and II in the parallel and perpendicular directions [32].

Parallel tensile and compressive failure mode:

$$F = \frac{\sigma_{11}^2}{X^2} + \frac{(\sigma_{12}^2 + \sigma_{13}^2)}{S_{\parallel}^2} \geq 1 \quad X$$

$$= \begin{cases} X_T & (\sigma_{11} > 0) \\ X_C & (\sigma_{11} < 0) \end{cases}, \quad F = \begin{cases} F_1 & (\text{Tensile}) \\ F_2 & (\text{Compressive}) \end{cases} \quad (1)$$

Perpendicular tensile and compressive failure mode:

$$F = \frac{(\sigma_{22} + \sigma_{33})^2}{Y^2} + \frac{(\sigma_{23}^2 - \sigma_{22}\sigma_{33})}{S_{\perp}^2} + \frac{(\sigma_{12}^2 + \sigma_{13}^2)}{S_{\parallel}^2} \geq 1$$

where $Y = \begin{cases} Y_T & ((\sigma_{22} + \sigma_{33}) > 0) \\ Y_C & ((\sigma_{22} + \sigma_{33}) < 0) \end{cases}$,

$$F = \begin{cases} F_3 & (\text{Tensile}) \\ F_4 & (\text{Compressive}) \end{cases} \quad (2)$$

with X_T, Y_T – Longitudinal and transverse tensile strength respectively

X_C, Y_C – Longitudinal and transverse compressive strength respectively

S_{\parallel}, S_{\perp} – Longitudinal and transverse shear strength respectively

F_1, F_2, F_3, F_4 - Failure index

Parallel damage evolution:

$$\text{Damage function } (d(\tau_{\parallel})) = \frac{d\max_{\parallel}}{B} \left[\frac{1+B}{1+Be^{-A(\tau_{\parallel}-\tau_{0\parallel})}} - 1 \right] \quad (3)$$

where

$$\text{Damage parameter } (A) = \tau_{0\parallel} L \left[\frac{1+B}{BG_{f\parallel}} \right] \log(1+B) \quad (4)$$

Strain energy threshold (τ_{\parallel})

$$= \begin{cases} \sqrt{\sigma_{11}^* \varepsilon_{11} + 2(\sigma_{12}^* \varepsilon_{12} + \sigma_{13}^* \varepsilon_{13})} & \varepsilon_{11} \geq 0 \\ \sqrt{2(\sigma_{12}^* \varepsilon_{12} + \sigma_{13}^* \varepsilon_{13})} & \varepsilon_{11} < 0 \end{cases} \quad (5)$$

Initial strain energy threshold ($\tau_{0\parallel}$)

$$= \tau_{\parallel} - \sqrt{E_{11}} \left[\frac{x-x_0}{L} \right] \quad (6)$$

Parallel fracture energy ($G_{f\parallel}$)

$$= \begin{cases} G_{f\parallel} \left(\frac{\sigma_{11}^2}{X_T^2} \right) + G_{f\parallel} \left(\frac{\sigma_{12}^2 + \sigma_{13}^2}{S_{\parallel}^2} \right) & \sigma_{11} \geq 0 \\ G_{f\parallel} \left(\frac{S_{\parallel}^2}{\sigma_{12}^2 + \sigma_{13}^2} \right) & \sigma_{11} < 0 \end{cases} \quad (7)$$

$$\text{Parallel fracture energy in mode I } (G_{f\parallel}) = C_1 K_{I\parallel}^2 \quad (8)$$

$$\text{Parallel fracture energy in mode II } (G_{f\parallel}) = C_1 K_{II\parallel}^2 \quad (9)$$

with Mode I – Stress intensity factor in parallel direction ($K_{I\parallel}$) $\approx 7K_{I\perp}$

Mode II – Stress intensity factor in parallel direction ($K_{II\parallel}$) $\approx 7K_{II\perp}$

B and $d\max_{II}$ – User defined parallel softening parameter and parallel maximum damage respectively

X and X_0 - Initial displacement and displacement at peak strength respectively.

L - Element length

Perpendicular damage evolution:

$$\text{Damage function } (d(\tau_{\perp})) = \frac{d\max_{\perp}}{D} \left[\frac{1+D}{1+De^{-C(\tau_{\perp}-\tau_{0\perp})}} - 1 \right] \quad (10)$$

where

$$\text{Damage parameter } (C) = \tau_{0\perp} L \left[\frac{1+D}{DG_{f\perp}} \right] \log(1+D) \quad (11)$$

Strain energy threshold (τ_{\perp})

$$= \begin{cases} \sqrt{\sigma_{22}^* \varepsilon_{22} + \sigma_{33}^* \varepsilon_{33} + 2\sigma_{23}^* \varepsilon_{23}} & \varepsilon_{22} + \varepsilon_{33} \geq 0 \\ \sqrt{2\sigma_{23}^* \varepsilon_{23}} & \varepsilon_{22} + \varepsilon_{33} < 0 \end{cases} \quad (12)$$

$$\text{Initial strain energy threshold } (\tau_{0\perp}) = \tau_{\perp} - \sqrt{E_{22}} \left[\frac{x-x_0}{L} \right] \quad (13)$$

Perpendicular fracture energy ($G_{f\perp}$)

$$= \begin{cases} G_{f\perp} \left(\frac{\sigma_{22}^2 + \sigma_{33}^2}{Y_T^2} \right) + G_{f\perp} \left(\frac{\sigma_{23}^2 - \sigma_{22}\sigma_{33}}{S_{\perp}^2} \right) & \sigma_{22} + \sigma_{33} \geq 0 \\ G_{f\perp} \left(\frac{S_{\perp}^2}{\sigma_{23}^2 - \sigma_{22}\sigma_{33}} \right) & \sigma_{22} + \sigma_{33} < 0 \end{cases} \quad (14)$$

Table 11. Initial elastic properties of poplar and okoume [36].

Material Properties	Elastic properties (MPa)									
	E11	E22	E33	G12	G13	G23	γ_{12}	γ_{13}	γ_{23}	ρ (kg/m3)
Poplar	10,900	1,003	469	818	752	120	0.392	0.318	0.329	480
Okoume	9,000	828	387	675	621	99	0.392	0.312	0.329	430
Ratios to E11		0.092	0.043	0.075	0.069	0.011				

$$\text{Perpendicular fracture energy in mode I } (G_{r_{I\perp}}) = C_I K_{I\perp}^2 \quad (15)$$

$$\text{Perpendicular fracture energy in mode II } (G_{r_{II\perp}}) = C_{II} K_{II\perp}^2 \quad (16)$$

$$C_I = \sqrt{\left(\frac{C_{11}C_{22}}{2}\right) \left[\left(\frac{C_{22}}{C_{11}}\right) + \left(\frac{2C_{12} + C_{66}}{2C_{11}}\right)\right]} \quad (17)$$

$$C_{II} = \left(\frac{C_{11}}{\sqrt{2}}\right) \sqrt{\left[\left(\frac{C_{22}}{C_{11}}\right) + \left(\frac{2C_{12} + C_{66}}{2C_{11}}\right)\right]} \quad (18)$$

$$C_{11} = \frac{1}{E_{11}}, C_{22} = \frac{1}{E_{22}}, C_{12} = \frac{-\nu_{11}}{E_{22}}, C_{66} = \frac{1}{G_{12}} \quad (19)$$

with $K_{I\perp}$ = Mode I – Stress intensity in perpendicular mode
 $K_{II\perp}$ = Mode II – Stress intensity in perpendicular mode
D and $d_{max_{II}}$ – User defined perpendicular softening parameter and perpendicular maximum damage respectively.
L – Element length
X and X_0 – Initial displacement and displacement at peak strength respectively.

3.2.2. Calibration of plywood core elastic behavior

The identification procedure was carried out with material constants from the literature [36] as shown in Table 11. Then each elastic constant was calculated from E_{11} according to a fixed ratio [36].

A numerical model for three point bending on a plywood structure without damage was used to calibrate the elastic behavior. For plywood core A, each ply of the core was meshed with 1,100 solid brick elements. ABAQUS (Implicit) was used for the simulation. As the sandwich plate geometry, boundary conditions and loading were symmetrical, only 1/4 of the specimen was computed. The final load was corrected by considering 4 times the calculated result. Figure 7 shows the quarter symmetric model considered. The top roller and bottom roller support were modeled with 900 and 1,800 solid elements respectively. A vertical displacement was applied to the top roller while the bottom one was clamped.

Then, a comparison was made with the results of three point bending experiments performed by the authors in [2]. A sensitivity study was performed to build an identification strategy. The sensitivity of each measurable quantity of each elastic constant was evaluated by considering a 10% increase. Table 12 presents results concerning the slope of the load/displacement curve for three and four point bending tests in the longitudinal and transverse directions and the ratio of

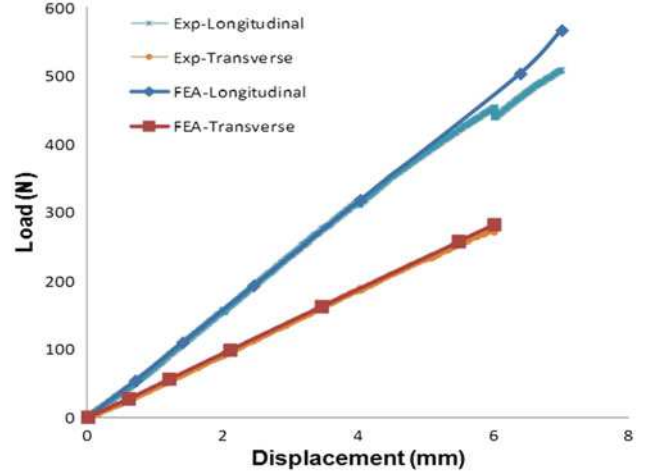


Figure 7. 3 point bending test on plywood A, force–displacement curve.

normal to longitudinal strain, which was obtained through digital image correlation used in three point bending tests on a lateral face of the sample near the plane of symmetry.

Finally, the longitudinal modulus of Okoume (E_{11}) had a significant influence on the predicted stiffness because of its top position which situated it farther from the neutral plane of the plywood structure. The Poisson ratio of Okoume (ν_{23}) was more sensitive to the predicted ratio of normal strain to longitudinal strain at the middle of the numerical model (see Table 12). The material properties identified are shown in Table 15, keeping the same ratios to E_{11} as presented in Table 11. The corresponding load/displacement numerical responses are compared to experimental results for longitudinal and transverse samples in Figure 7.

3.2.3. Calibration of plywood core plastic behavior and aluminum skin elasto-plastic behavior

For plywood structures with aluminum skin, debonding, transverse shear and fiber fracture were identified as the predominant failure modes under low-velocity impact [6]. In order to simulate and represent the above failure modes along with non-linear behavior of the skin, the aluminum skin of the sandwich structure was modeled with material model MAT_98 (Simplified Johnson Cook) of the LS-DYNA software, without including thermal effects on the behavior. Johnson Cook expresses the flow stress through the following equation. Failure occurs when the effective plastic strain exceeds $\bar{\epsilon}^P$.

$$\sigma_y = (A + B\bar{\epsilon}^{Pn}) \left(\frac{1 + C \ln \dot{\bar{\epsilon}}}{\dot{\bar{\epsilon}}_0} \right) \quad (20)$$

where A and B are input constants, C is strain rate sensitivity, n is the strain hardening factor, $\bar{\epsilon}^P$ is the maximum

Table 12. Sensitivity analysis on material parameters of plywood layers.

Properties		Plywood – 3-Point bending			
		Longitudinal		Transverse	
		% of increase in slope	% error in strain ratio ($\epsilon_{33}/\epsilon_{11}$)	% of increase in slope	% error in strain ratio ($\epsilon_{33}/\epsilon_{11}$)
E11	Poplar	35.57		2.35	
	Okoume	48.03		77.76	
E22	Poplar	0.29		5.28	
	Okoume	4.03		9.03	
E33	Poplar	0.43		0.22	
	Okoume	1		0.24	
ν_{12}	Poplar	0°	22.27		21.76
		90°	98.38		89.51
	Okoume	0°	8.83		28.67
		90°	39.72		44.69
ν_{13}	Poplar	0°	77.62		53.41
		90°	11.27		18.17
	Okoume	0°	75.54		78.77
		90°	69.06		72.35
ν_{23}	Poplar	0°	18.13		15
		90°	52.18		91.62
	Okoume	0°	12.73		33.87
		90°	144.85		125.82
G12	Poplar	0		0	
	Okoume	0		0.02	
G13	Poplar	0.8		0.39	
	Okoume	0.38		0.14	
G23	Poplar	6.59		3.29	
	Okoume	1.8		0.05	

Table 13. Initial damage properties (Plywood A).

Materials	Failure stresses (MPa) – (Hashin damage)						Fracture energy (N/mm)			
	σ_{lt}	σ_{lc}	σ_{tt}	σ_{tc}	σ_{ls}	σ_{ts}	Perpendicular		Parallel	
							$G_{LR(I)}$ - Tension	$G_{LR(II)}$ - Shear	$G_{LT(I)}$ - Tension	$G_{LT(II)}$ - Shear
Poplar	109.6	38.2	3.4	3.7	6.2	8.2	0.40	8.3	20.1	41.4
Okoume	103.6	36.1	3.2	3.5	5.8	7.8	0.34	6.9	16.7	34.9

Table 14. Initial plastic damage properties for aluminum [40].

E (GPa)	ν	A (GPa)	B (GPa)	n (hardening parameter)	C (Strain rate-constant)	ϵ_p (Maximum plastic strain)	σ_{ult} (GPa)
75	0.3	0.28	0.68	0.53	0.001	0.8	0.116

effective plastic strain, $\dot{\epsilon}$ is the maximum effective plastic strain rate, and ϵ_0 is the reference strain rate.

The law was calibrated in the same way as for plywood alone, using the results in bending obtained for plywood with aluminum skins [2] and an explicit finite element model including damage to calibrate elastic and plastic behavior of the skins. The same geometry as Figure 7, with a quarter of the symmetric model, was considered. Here, each aluminum skin was modeled with two layers of solid elements through the thickness while continuum shell elements were used for the plywood core. We used the calibrated elastic properties obtained from the previous model for the plywood core and initiated the identification process with damage property data from the literature for both the plywood core [32, 36 and 39] and the skins [28] (see Tables 13 and 14). Then we identified plastic and damage properties for both the plywood core and aluminum skins after a sensitivity study on the three point bending test. The final elastic damage properties are shown in Table 15.

Figure 8 compares the numerical model (with improved materials data (see Table 15)) and experimental load/displacement responses for longitudinal and transverse samples

of plywood structures with aluminum skin. Good correlation can be seen in terms of initial slope, stiffness loss and maximum load for both longitudinal and transverse samples. On the other hand, failure of the sample is not captured by the model.

3.2.4. Cohesive layer behavior

For cohesive layers, cohesive mixed mode MAT_138 was used in order to simulate delamination and debonding between skins and core. Mixed mode cohesive behavior is now commonly used for modeling delamination as in [14, 15]. The law is shown Figure 9, using the following equations.

$$\delta^F = \frac{2(1 + \beta^2)}{\delta^0} \left[\left(\frac{EN}{GIC} \right)^{X_{MU}} + \left(\frac{ET \times \beta^2}{GIIC} \right)^{X_{MU}} \right]^{-\frac{1}{X_{MU}}} \quad (21)$$

$$\delta^0 = \delta_I^0 \delta_{II}^0 \sqrt{\left(\frac{1 + \beta^2}{(\delta_{II}^0)^2 + (\beta \delta_{II}^0)^2} \right)} \quad (22)$$

Table 15. Nonlinear and damage properties of plywood, aluminum and composite skins, and cohesive layers.

Elastic properties (GPa)											
Panels	Materials	E ₁₁	E ₂₂	E ₃₃	G ₁₂	G ₁₃	G ₂₃	ν ₁₂	ν ₁₃	ν ₂₃	ρ (kg/m ³)
Ply - A	Poplar	9.50	0.87	0.87	0.66	0.69	0.11	0.392	0.318	0.329	480
	Okoume	8.00	0.74	0.74	0.55	0.60	0.09	0.392	0.318	0.329	430
Ply - B	Poplar	5.50	0.51	0.51	0.38	0.40	0.06	0.162	0.318	0.329	480
	Okoume	3.50	0.32	0.32	0.24	0.26	0.04	0.162	0.318	0.329	430
Ply - A / Carbon	Carbon	138	6.39	6.39	4.69	4.69	2.3	0.346	0.346	0.4	1,420
Ply - A / Glass	Glass	87	4.03	4.03	2.96	2.96	1.45	0.216	0.216	0.366	1,850
Ply - B / Flax	Flax	25	25	3.44	1.27	1.24	1.23	0.4	0.397	0.5	1,500

Failure stresses: wood and composite plies (GPa)											
Panels	Materials	σ _{Lt}	σ _{Lc}	σ _{Tt}	σ _{Tc}	σ _{Nt}	σ _{Nc}	σ _{Ls}	σ _{Ts}	σ _{Ns}	
Ply -A	Poplar	0.080	0.028	0.002	0.003	-	-	0.004	0.006	-	
	Okoume	0.074	0.026	0.002	0.002	-	-	0.004	0.006	-	
Ply -B	Poplar	0.110	0.038	0.003	0.004	-	-	0.006	0.008	-	
	Okoume	0.104	0.036	0.003	0.004	-	-	0.006	0.008	-	
Ply - A / Carbon	Carbon	1.84	1.01	0.038	0.234	0.038	0.59	0.042	0.042	0.042	
Ply - A / Glass	Glass	1.69	0.924	0.035	0.215	0.035	0.542	0.039	0.039	0.039	
Ply - B / Flax	Flax	0.933	0.509	0.019	0.119	0.019	0.296	0.021	0.021	0.021	

Elastic and Johnson-Cook law parameter (aluminum skin)											
Panels	Materials	E (GPa)	ν	A (GPa)	B (GPa)	n	C (Strain rate)	ε _p	σ _{ult} (GPa)	ρ (kg/m ³)	
Ply - A / Al	Aluminum	65	0.33	0.028	0.068	0.2	0.0054	0.21	0.116	2,700	

Cohesive properties (Epoxy type resin)											
Materials	K _I (kN/mm ³)	K _{II} (kN/mm ³)	σ _N (GPa)	σ _S (GPa)	G _{IC} (J/m ²)	G _{IIC} (J/m ²)	XMU	ρ (kg/m ³)			
Cohesive (Epoxy)	100	100	0.06	0.06	765	1,250	1	1,170			

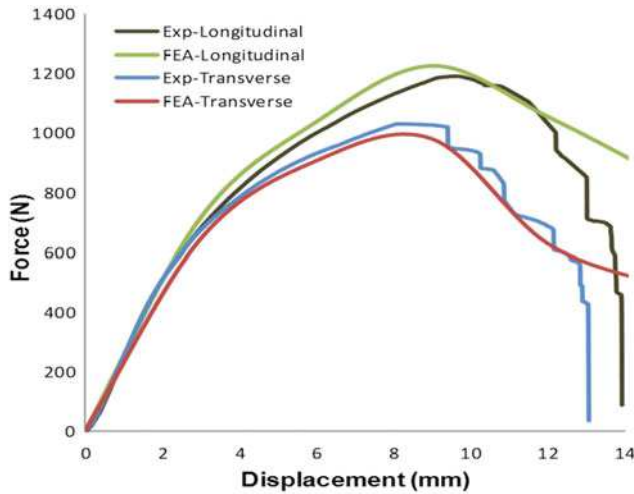


Figure 8. Force–displacement curve (plywood A/aluminum skins) - 3 point bending.

where

$$\delta_I^0 = \frac{T}{EN}, \delta_{II}^0 = \frac{TS}{ET}, \beta = \frac{\delta_{II}}{\delta_I}$$

with T and S the Peak tractions in the normal and tangential directions respectively, EN and ET the unit stiffness in the normal and tangential directions, respectively, and G_{IC} and G_{IIC} the critical energy release rates in mode I and mode II respectively.

XMU – the exponent of mixed mode criteria – was set to 1 in accordance with [14, 15]

δ^F is the ultimate mixed-mode displacement.

The cohesive behavior presented in Table 15, in which values are taken from [40], will be used for interfaces inside composite skins or between skins and plywood encountered in this work. Of course, better accuracy would be obtained

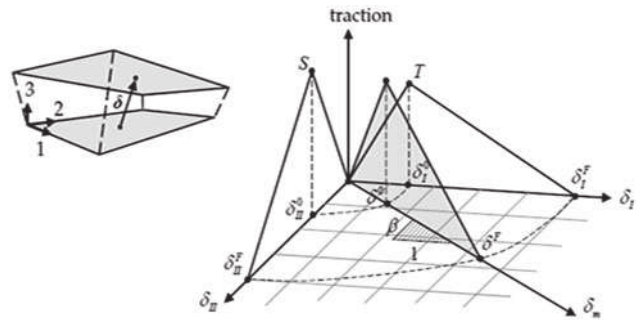


Figure 9. Mixed mode cohesive behavior.

with a finer identification of each interface property inside the plywood and of each skin.

3.2.5. Composite skin damage behavior

For plywood structures with composite skins, delamination, transverse shear of the core, fiber fracture, debonding and matrix cracking were identified as predominant failure modes under low-velocity/low-energy impact. Several material models are available in LS-DYNA to model continuous fiber composite laminate. Each material model utilizes a different model strategy to predict failure initiation, and for material properties and degradation schemes. The material model used in this study is an orthotropic material model that takes the maximum stress failure criterion for tension failure, compressive failure, shear failure and delamination. This material model has been used to simulate impact and crash response of thick composite structures with solid elements. Each failure mode is classified according to the fiber direction. (Here, the subscripts 1, 2, and 3 denote the longitudinal, transverse, and normal directions). The failure criterion of this material model is given as follows:

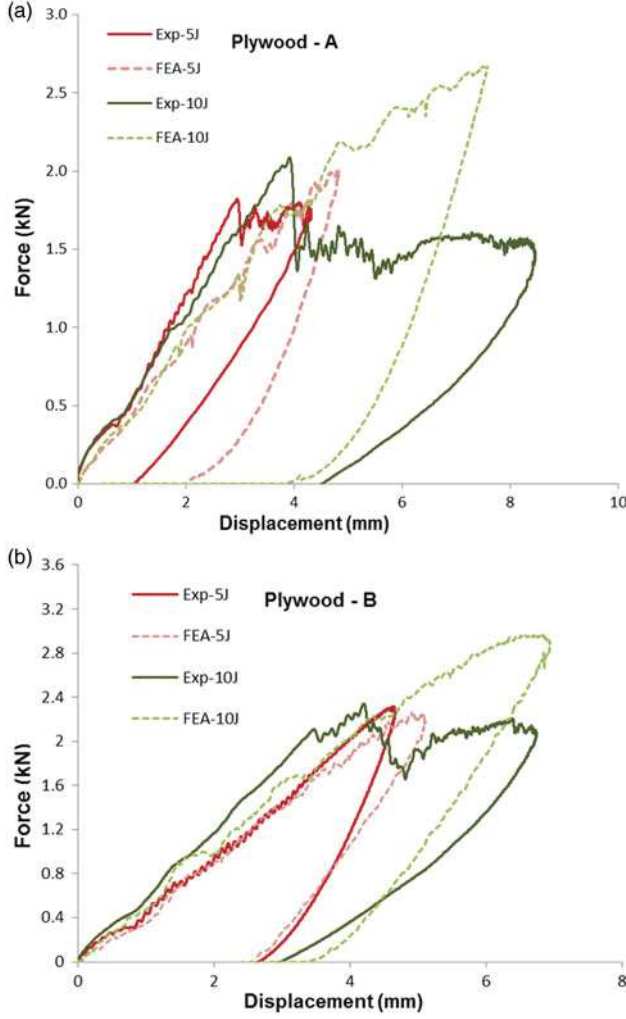


Figure 10. Force-displacement plot at 5 J, 10 J – (a) plywood A, (b) plywood B.

Longitudinal and transverse tensile mode:

$$F = \left(\frac{\sigma}{X}\right)^2 + \left(\frac{\sigma_{12}}{S_{12}}\right)^2 + \left(\frac{\tau}{S}\right)^2 \geq 1 \quad (23)$$

where

$$\begin{cases} X = X_T, \sigma = \sigma_{11}, \tau = \sigma_{13}, S = S_{13}, F = F_1 (\sigma_{11} > 0) (L) \\ X = Y_T, \sigma = \sigma_{22}, \tau = \sigma_{23}, S = S_{23}, F = F_2 (\sigma_{22} > 0) (T) \end{cases}$$

Through thickness shear mode (longitudinal and transverse):

$$F = \left(\frac{\sigma}{X}\right)^2 + \left(\frac{\tau}{S}\right)^2 \geq 1 \begin{cases} X = X_T, \sigma = \sigma_{11}, \tau = \sigma_{13}, S = S_{13}, F = F_3 (L) \\ X = Y_T, \sigma = \sigma_{22}, \tau = \sigma_{23}, S = S_{23}, F = F_4 (T) \end{cases} \quad (24)$$

Delamination mode (through thickness tensile):

$$F_5 = \left(\frac{\sigma_{33}}{Z_T}\right)^2 + \left(\frac{\sigma_{23}}{S_{23}}\right)^2 + \left(\frac{\sigma_{13}}{S_{13}}\right)^2 \geq 1 (\sigma_{33} > 0) \quad (25)$$

Longitudinal compression mode:

$$F_6 = \left(\frac{\sigma_{11}}{X_C}\right)^2 \geq 1 (\sigma_{11} < 0) \quad (26)$$

Transverse compression mode:

$$F_7 = \left(\frac{\sigma_{22}}{S_{12} + S_{23}}\right)^2 + \left[\left(\frac{Y_C}{S_{12} + S_{23}}\right)^2 - 1\right] \left(\frac{\sigma_{22}}{|Y_C|}\right) + \left(\frac{\sigma_{12}}{S_{12}}\right)^2 + \left(\frac{\sigma_{23}}{S_{23}}\right)^2 \geq 1 (\sigma_{22} < 0) \quad (27)$$

Through thickness compression mode:

$$F_8 = \left(\frac{\sigma_{33}}{S_{13} + S_{23}}\right)^2 + \left[\left(\frac{Z_C}{S_{13} + S_{23}}\right)^2 - 1\right] \left(\frac{\sigma_{33}}{|Z_C|}\right) + \left(\frac{\sigma_{13}}{S_{13}}\right)^2 + \left(\frac{\sigma_{23}}{S_{23}}\right)^2 \geq 1 (\sigma_{33} < 0) \quad (28)$$

We used the calibrated elastic properties obtained from the previous model for the plywood core and initiated the identification process of elastic and damage properties data from the literature [40] for the composite skins. Unlike plywood A, where elastic constants were identified on the 3 point bending test, plywood B and the composite skin had data constants directly identified from the impact test (initiating the identification from plywood A properties). The calibrated data constants for different composite skins are summarized in Table 15.

4. Comparisons with experimental results

4.1. Case of impacts on plywood a and B alone

The experimental and numerical contact laws for the plywood structures alone, impacted under 5 J and 10 J, are shown in Figure 10a and b. At 15 J, correlation is not possible due to perforation. Globally, the numerical prediction is rather good for both plywoods and for 5 J impact, which means that the elastic values were correctly estimated and the damage extension was small. The results are considerably less accurate for 10 J in terms of peak load, energy absorbed, final failure and unloading prediction (see also Table 16). So, further investigations are needed to characterize plywood and plywood component damage parameters and thus enhance the model description.

A comparison ply by ply can also be proposed and the case of 10 J impact for plywood A is shown in Figure 11. Since the error in residual indentation depth in this case is only 16% (Table 16), the proposed numerical model can correctly predict the position of maximum plastic deformation, as well as permanent indentation, in the specimens. This also shows that the rough hypothesis made in this study can be accurate enough to model the out-of-plane behavior of the plywood alone.

4.2. Case of impacts on plywood a core and aluminum skin

In the cases of sandwich structures using plywood A core and aluminum skin, a simulation was performed of the impact tests for the three energy levels. The correlation between experimental and numerical results was satisfactory,

Table 16. Comparison of predicted impact parameters for different wooden sandwich structures (gray cells: Perforation).

Materials	Energy level (J)	Initial slope			Peak Load (kN)			Maximum deflection (mm)			Permanent indentation (mm)			Absorbed Energy (J)				
		Exp.	FEM	% Error	Exp.	FEM	% Error	Exp.	FEM	% Error	Exp.	FEM	% Error	Exp.	FEM	% Error		
Plywood - A	5	0.60	0.45	33	1.82	2.01	9	4.32	4.83	11	1.19	2.13	44	2.49	2.93	15		
	10	0.52	0.45	16	2.09	2.67	22	8.46	7.58	12	4.52	3.88	16	8.81	7.80	13		
	15	–	–	–	–	–	–	–	–	–	–	–	–	–	–	–		
Plywood - B	5	0.49	0.49	0	2.31	2.26	2	4.60	5.11	10	2.81	2.60	8	3.52	3.21	10		
	10	0.59	0.53	11	2.51	2.95	15	6.74	6.95	3	2.99	3.44	13	7.13	5.85	22		
	15	–	–	–	–	–	–	–	–	–	–	–	–	–	–	–		
Plywood - A/Aluminium	5	0.91	1.22	25	3.00	3.02	1	3.29	3.30	0	2.02	2.31	13	3.68	4.90	25		
	10	0.87	1.20	28	4.03	3.99	1	4.91	4.64	6	3.65	3.80	4	8.97	10.28	13		
	15	0.86	1.17	26	4.60	4.37	5	6.01	5.65	6	4.73	4.17	13	12.33	14.96	18		
Vacuum Moulding	Plywood -A /Glass	5	1.09	1.16	6	3.45	3.54	3	2.97	3.06	3	0.90	1.38	35	3.05	3.41	11	
		10	1.05	1.28	18	4.33	4.62	6	4.42	4.18	6	2.07	1.96	6	8.10	7.28	11	
		15	1.15	1.27	9	4.95	5.09	3	5.22	4.56	14	2.09	2.30	9	10.65	8.57	24	
	Plywood -A/Carbon	5	1.15	1.30	12	3.71	3.68	1	3.04	2.98	2	0.53	1.13	53	2.82	3.45	18	
		10	1.17	1.34	13	4.77	4.91	3	4.19	4.04	4	1.00	1.72	42	5.67	7.22	21	
		15	1.24	1.35	8	4.51	5.64	20	5.47	4.93	11	1.35	2.55	47	9.75	10.90	11	
	Thermo compression	Plywood -B /Flax	5	0.78	0.86	9	2.72	2.74	1	2.55	2.59	2	1.80	1.76	2	3.45	3.34	3
			10	0.75	0.81	7	3.68	3.75	2	5.11	5.20	2	2.33	2.31	1	7.39	6.16	20
			15	0.73	0.85	14	4.02	4.27	6	6.49	6.56	1	2.80	3.94	29	12.20	8.85	38
Plywood -B /Carbon		5	0.84	1.17	28	3.69	3.60	3	3.36	3.19	5	0.90	1.17	23	2.89	3.32	13	
		10	1.41	1.30	8	5.34	5.23	2	3.85	4.28	10	0.70	1.49	53	5.50	7.35	25	
		15	1.24	1.33	7	6.31	6.07	4	5.02	5.12	2	1.20	2.29	48	8.26	10.53	22	
Plywood -B / Glass		5	1.16	1.33	13	3.51	3.54	1	2.91	3.14	7	0.66	1.81	64	2.86	4.00	29	
		10	1.10	1.29	15	4.34	4.37	1	4.25	4.15	2	1.61	2.61	38	6.98	7.44	6	
		15	1.05	1.31	20	4.98	5.15	3	5.67	4.81	18	2.73	2.88	5	12.06	10.94	10	

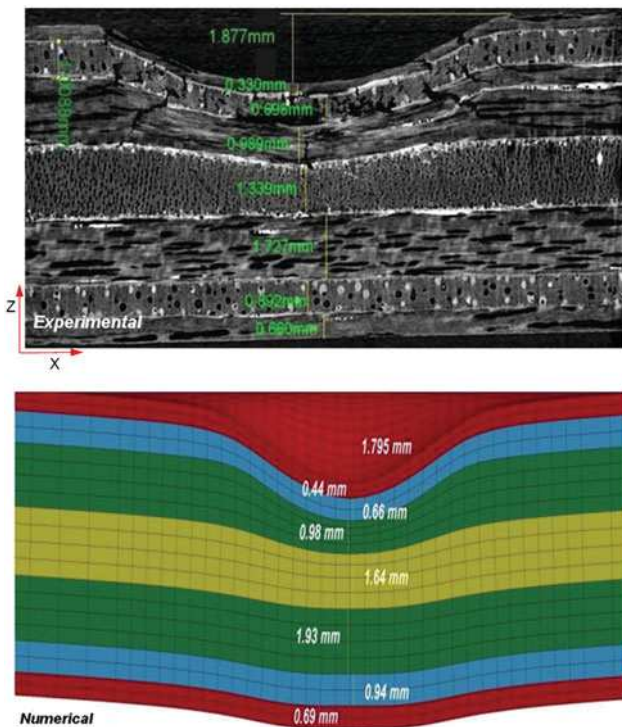


Figure 11. Comparison of crushing for plywood -A at 10 J (a) experimental, (b) numerical.

as shown in Figure 12, where experimental and numerical curves are very similar. This is probably due to the plastic behavior of the skins, which is simple to model. The indentation depth and the crushing of each ply are correctly estimated, as is the absorbed energy, with an error of between 5 and 15% (Table 16 and Figure 13).

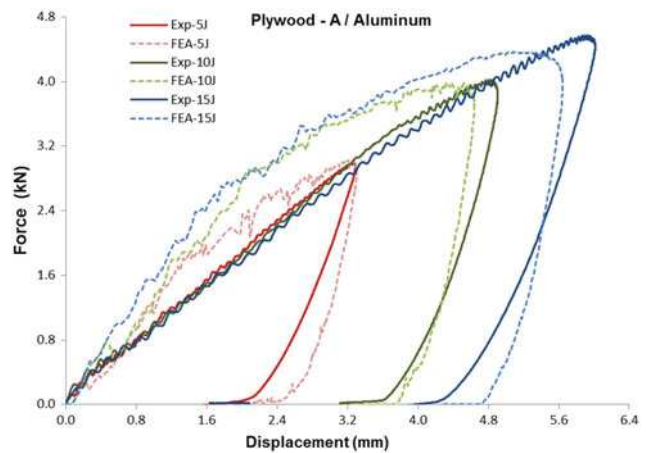


Figure 12. Force–displacement plot at 5 J, 10 J and 15 J (plywood A/aluminium skin).

4.3. Case of impacts on plywood a and B core and carbon skin

Regarding the sandwich structures with plywood A and B cores and carbon skins, good correlation was obtained in terms of the peak load, initial slope and unloading portion under 5J and 10J impact energy (see Figures 14 and 15 and Table 16). In particular, the results for maximum deflection and failure by plywood crushing under the skin predicted by numerical simulation were practically the same as those measured in the tests (see Figure 16). However, the permanent indentation was difficult to capture due to the elastic behavior of the skin after impact. However, at this stage of development, the model is able to capture the complex behavior involved [3]. Concerning the simulation of the impact tests at 15J, good correlation was obtained in the

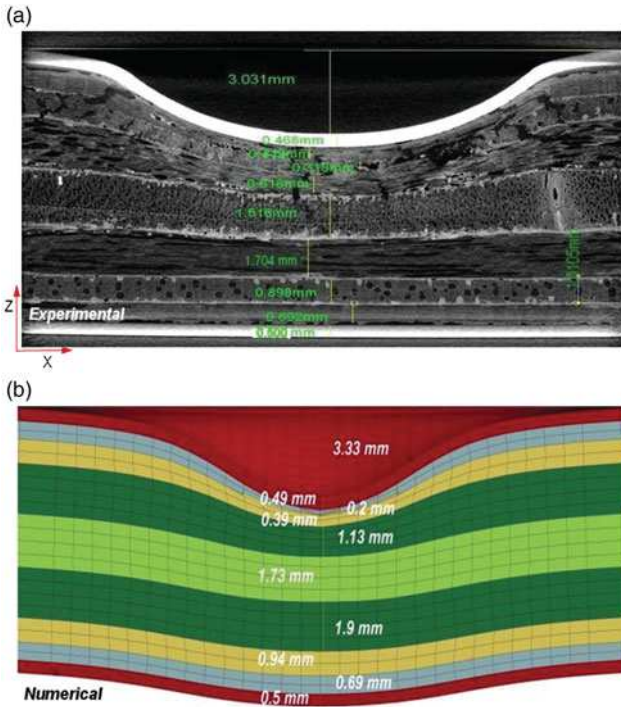


Figure 13. Comparison of plastic deformation and indentation for (plywood a/ aluminum skin) (a) experimental, (b) numerical.

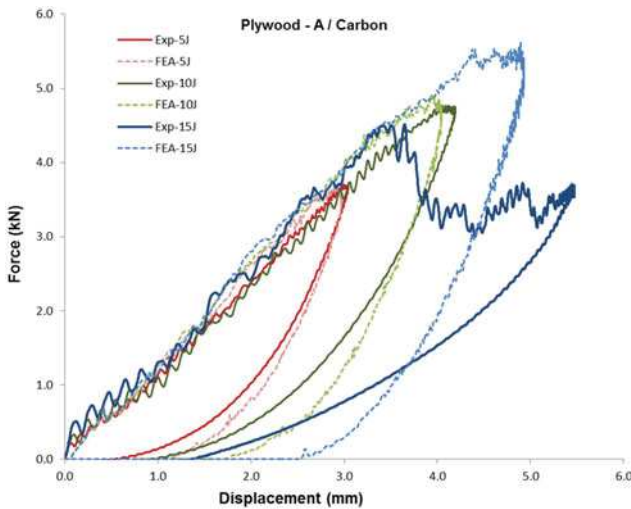


Figure 14. Force-displacement plot at 5 J, 10 J and 15 J (plywood - A/ carbon skins).

initial slope and indentation but not in peak load, maximum deflection and unloading portion. With experimental results, we encounter delamination and a spring back effect of the skin with almost no visible indentation at 15J while marked indentation and delamination is visible at the interface between the core and the top skin (Figure 16). These differences can be explained by poor adhesion between skins and core being obtained in the manufacturing process. The failure of the numerical model to represent this spring back and marked delamination was probably due to a difference between the interface properties and the cohesive behavior used in the simulation. Here, more thorough investigation should be conducted during the manufacturing process to improve the adhesion of the skins or identification of the

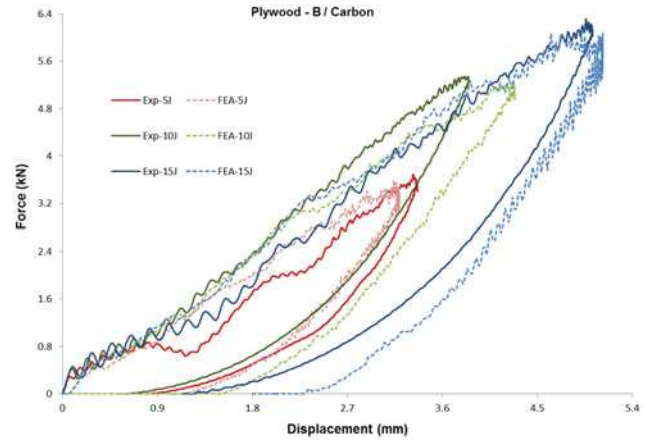


Figure 15. Force-displacement plot at 5 J, 10 J and 15 J (plywood - B/ carbon skins).

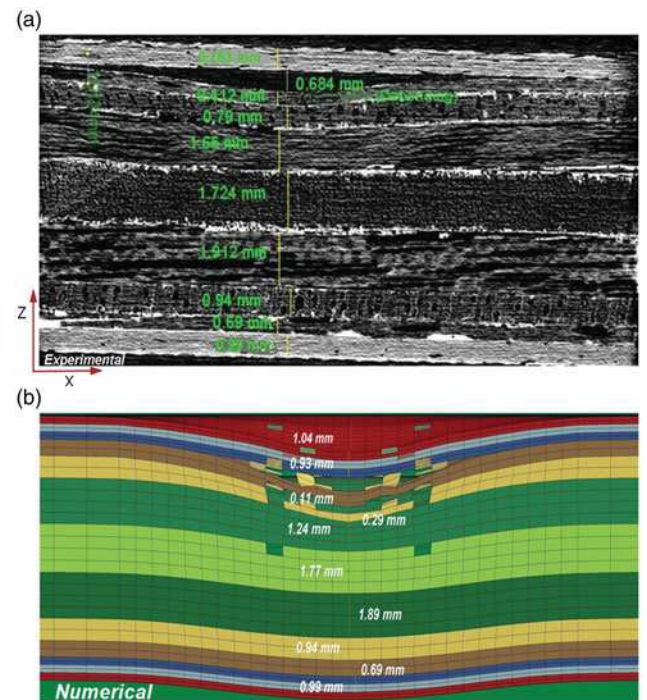


Figure 16. Comparison of plastic deformation and indentation for (plywood - A/ carbon skins) (a) experimental, (b) numerical.

cohesive behavior should be compulsory in the numerical model. When the sandwich core was plywood B, excellent correlation between experimental and numerical tests was obtained in terms of initial slope, peak load and maximum deflection at all impact energy levels (see Figure 15 and Table 16) which may be explained by better adhesion being obtained in the thermo-compression process in the case of plywood B/ carbon skin and the absence of local delamination under the impactor.

4.4. Case of impacts on plywood a and B cores and glass skins

For the sandwich structures with plywood cores (A or B) and glass skins, impact tests at energy levels of 5J and of 10J showed good correlation in terms of peak load, initial

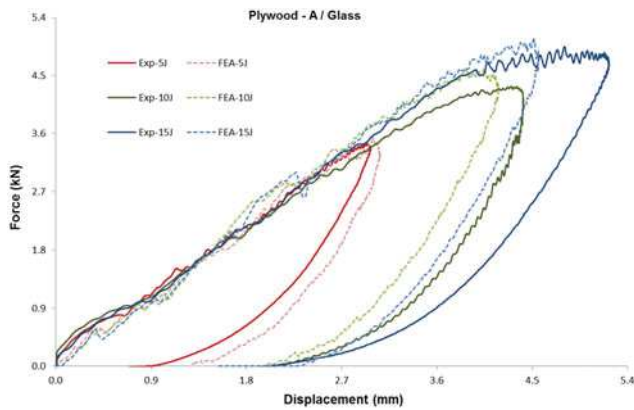


Figure 17. Force–displacement plot at 5 J, 10 J and 15 J (plywood A/ glass skins).

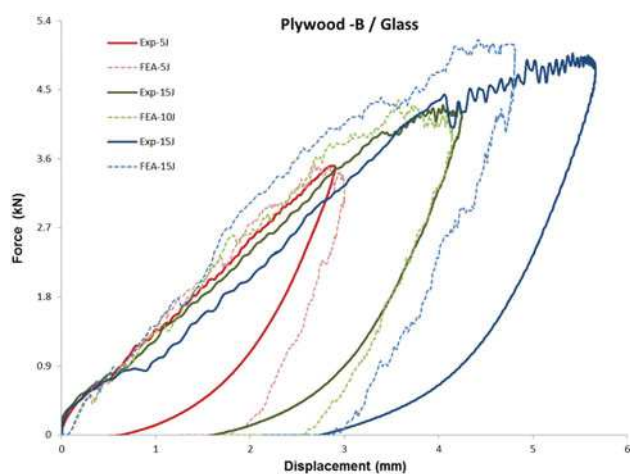


Figure 18. Force–displacement plot at 5 J, 10 J and 15 J (plywood B/ glass skins).

slope, maximum deflection and indentation (see Figures 17, 18 and Table 16). Maximum plastic deformation was located at one-third of the sample thickness (see Figure 19a and b). The conclusion is the same for both numerical and experimental cases. In the cases of impact energies of 10 J and of 15 J, the prediction by the numerical model, in terms of failure modes, position of the maximum plastic deformation, initial slope and peak load were confirmed by experimental measurement, but moderate correlation was obtained in terms of unloading and absorbed energy, which may have been due to the better adhesion obtained in thermo-compression process. However, regarding permanent indentation, poor correlation was obtained between numerical and experimental results. These remarks may describe a mismatch between interface properties and the cohesive behavior used in the simulation. As explained above, the cohesive behavior of the interfaces needs further calibration.

4.5. Case of impacts on plywood B core and flax skins

For the sandwich structures with plywood core B and flax skin, maximum plastic deformation occurred up to the middle section of samples in both numerical and experimental test cases (see Figure 20 and Table 16). Moreover, similar failure modes, such as fiber fracture, were found at higher

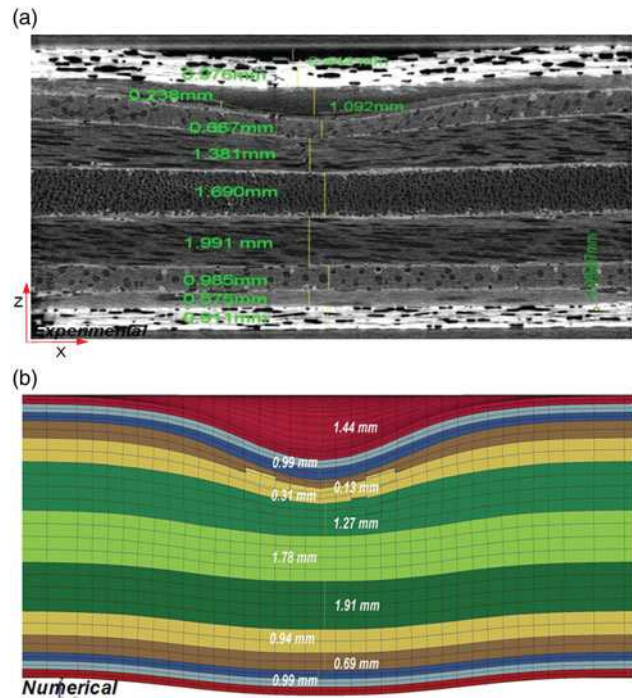


Figure 19. Comparison of plastic deformation and indentation for (plywood A/ glass skins) (a) experimental, (b) numerical.

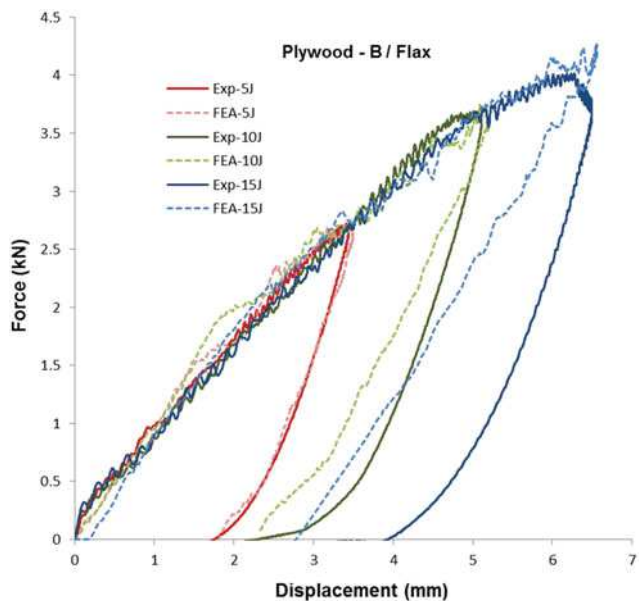


Figure 20. Force–displacement plot at 5 J, 10 J and 15 J (plywood – B/ flax skins).

energy levels in experimental tests and in numerical simulation (Figure 20). Good correlation was obtained for the peak load, initial slope, the position of the maximum plastic deformation in the tested specimen, maximum deflection, and indentation at all impact energy levels (Figure 21 and Table 16). However, weak correlation was obtained in terms of the unloading portion at 10 J and 15 J, which may be explained by insufficient progressive material damage modeling in LS-DYNA and incomplete realization of bouncing in simply supported boundary conditions in the numerical model.

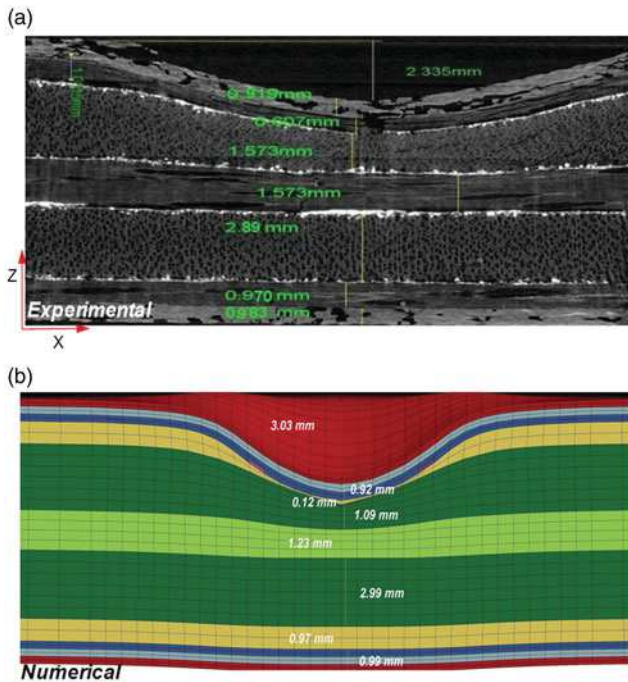


Figure 21. Comparison of plastic deformation and indentation for plywood – A/glass skins (a) experimental, (b) numerical.

5. Conclusions

A numerical model of sandwich structures with plywood cores has been developed to model low velocity, low energy impacts on these structures. Nine configurations were studied at 3 levels of energy. The model uses available material laws for plywood, composite and metallic skins. Due to the large number of materials contained in the plywood and in the skins, and the number of damage parameters involved, only a rough estimation of the material properties was made. Despite this drawback, the model can predict the impact behaviors correctly, especially for 5 J and 10 J impacts, where damage is limited. Most of the errors in the experimental and numerical results in terms of initial slope, peak load and maximum deflections are lower than 20%. The error in terms of permanent indentation is larger due to the complex behavior involved [41], which is not taken into account correctly in the model. The difference is also more significant in terms of absorbed energy. Material damage model in LS-DYNA does not integrate enough softening effects in the damage process, and some improvements will have to be proposed in order to obtain better correlation. In addition, exhaustive nonlinear characterization and the use of more advanced modeling strategies [14–19] would be relevant. The numerical strategy proposed in this paper is a first approach to highlight the difficulties of impact modeling of these materials with a classical approach available in commercial software.

References

[1] D. Zenkerts, *The Handbook of Sandwich Construction*. West Midlands: Engineering Materials Advisory Services Ltd, 1997.
 [2] J. Susainathan, F. Eyma, E. De Luycker, A. Cantarel, and B. Castanié, “Manufacturing and quasi-static bending behavior of

wood-based sandwich structures,” *Compos. Struct.*, vol. 182, pp. 487–504, 2017.

- [3] S. Abrate, B. Castanié, and Y. D. S. Rajapakse, *Dynamic Failure of Composite and Sandwich Structures*. Berlin: Springer 2013.
 [4] J. Tomblin, T. Lacy, B. Smith, S. Hooper, A. Vizzini, and S. Lee, “Review of damage tolerance for composite sandwich airframe structures” FAA Report Number DOT/FAA/AR-99/49.
 [5] B. Castanié, Y. Aminanda, C. Bouvet, and J. J. Barrau, “Core crush criteria to determine the strength of sandwich composite structures subjected to compression after impact,” *Compos. Struct.*, vol. 86, no. 1–3, pp. 243–250, 2008.
 [6] J. Susainathan, F. Eyma, E. De Luycker, A. Cantarel, and B. Castanié, “Experimental investigation of impact behavior of wood-based sandwich structures,” *Compos. Part A*, vol. 109, pp. 10–19, 2018.
 [7] Y. Aminanda, B. Castanie, J. J. Barrau, and P. Thevenet, “Experimental analysis and modeling of the crushing of honeycomb cores,” *Appl. Compos. Mater.*, vol. 12, no. 3–4, pp. 213–217, 2005.
 [8] B. Castanié, C. Bouvet, Y. Aminanda, J. J. Barrau, and P. Thevenet, “Modelling of low energy/low velocity impact on nomex honeycomb sandwich structures with metallic skins,” *Int. J. Impact Eng.*, vol. 35, no. 7, pp. 620–634, 2008.
 [9] J. De Lorna, M. Gibson, and F. Ashby, *Cellular Solids: Structures and Properties*. Cambridge, MA: Cambridge University Press.
 [10] S. Long, X. Yao, H. Wang, and X. Zhang, “Failure analysis and modeling of foam sandwich laminates under impact loading,” *Compos. Struct.*, vol. 197, pp. 10–20, 2018.
 [11] R. Olsson, and T. B. Block, “Criteria for skin rupture and core shear cracking induced by impact on sandwich panels,” *Compos. Struct.*, vol. 125, pp. 81–87, 2015.
 [12] S. Abrate, “Criteria for yielding or failure of cellular materials,” *J. Sandwich Struct. Mater.*, vol. 10, no. 1, pp. 5–51, 2008.
 [13] J. Aubry *et al.*, “Change of scale strategy for the microstructural modelling of polymeric rohocell foams,” *Comput. Mater. Continua*, vol. 39, pp. 21–47, 2014.
 [14] C. Bouvet, B. Castanié, M. Bizeul, and J. J. Barrau, “Low velocity impact modelling in laminated composite panels with discrete interface elements,” *Int. J. Solids Struct.*, vol. 46, no. 14–15, pp. 2809–2821, 2009.
 [15] V. Achard, C. Bouvet, B. Castanié, and C. Chirol, “Discrete ply modelling of open hole tensile tests,” *Compos. Struct.*, vol. 113, pp. 369–381, 2014.
 [16] F. Pascal, O. Dorival, P. Navarro, S. Marguet, and J. F. Ferrero, “Impact damage prediction in thin woven composite laminates—part I: modeling strategy and validation,” *Compos. Struct.*, vol. 190, pp. 32–42, 2018.
 [17] B. Y. Chen, S. T. Pinho, N. V. De Carvalho, P. M. Baiz, and T. E. Tay, “A floating node method for the modelling of discontinuities in composites,” *Eng. Fracture Mech.*, vol. 127, pp. 104–134, 2014.
 [18] X. Lu, B. Y. Chen, V. B. C. Tan, and T. E. Tay, “A separable cohesive element for modelling coupled failure in laminated composite materials,” *Compos. Part A*, vol. 107, pp. 387–398, 2018.
 [19] M. Naderi, J. Jung, and Q. Yang, “A three dimensional augmented finite element for modeling arbitrary cracking in solids,” *Int. J. Fracture*, vol. 197, no. 2, pp. 147–168, 2016.
 [20] D. W. Sleight, *Progressive Failure Analysis Methodology for Laminated Composite Structures*, and NASA/TP-1999-209107. Hampton, VA: Nasa LRC, 1999.
 [21] N. Murugesan, and V. Rajamohan, “Prediction of progressive ply failure of laminated composite structures: a review,” *Arch. Comput. Methods Eng.*, vol. 24, no. 4, pp. 841–853, 2017.
 [22] C.-S. Lee, J.-H. Kim, S.-K. Kim, D.-M. Ryu, and J.-M. Lee, “Initial and progressive failure analyses for composite laminates using puck failure criterion and damage-coupled finite element method,” *Compos. Struct.*, vol. 121, pp. 406–441, 2015.

- [23] D. C. Pham, X. S. Sun, V. B. C. Tan, B. Chen, and T. E. Tay, "Progressive failure analysis of scaled double-notched carbon/epoxy composite laminates," *Int. J. Damage Mech.*, vol. 21, no. 8, pp. 1154–1185, 2012.
- [24] D. Du, Y. Hu, H. Li, C. Liu, and J. Tao, "Open-hole tensile progressive damage and failure prediction of carbon fibre-reinforced PEEK-titanium laminates," *Compos. Part B*, vol. 91, pp. 65–74, 2016.
- [25] C. Adalian, and P. Morlier, "A model for the behavior of wood under multiaxial compression," *Compos. Sci. Technol.*, vol. 20, pp. 404–408, 2001.
- [26] T. Polocoş, B. Kasal, and F. Stöckel, "State-of-the-art: intermediate and high strain rate testing of solid wood," *Wood Sci. Technol.*, vol. 51, no. 6, pp. 1479–1534, 2017.
- [27] F. Chen *et al.*, "Impact properties of bamboo bundle laminated veneer lumber by preprocessing densification technology," *J Wood Sci.*, vol. 60, no. 6, pp. 421–427, 2014.
- [28] H. Wang, K. R. Ramakrishnan, and K. Shankar, "Experimental study of the medium velocity impact response of sandwich panels with different cores," *Mater. Design*, vol. 99, pp. 68–82, 2016.
- [29] N. Jover, B. Shafiq, and U. Vaidya, "Ballistic impact analysis of balsa core sandwich composites," *Compos. Part B*, vol. 67, pp. 160–169, 2014.
- [30] B. Toson, P. Viot, and J. J. Pesqué, "Finite element modeling of balsa wood structures under severe loadings," *Eng. Struct.*, vol. 70, pp. 36–52, 2014.
- [31] M. Vural, and G. Ravichandran, "Dynamic response and energy dissipation characteristics of balsa wood: experiment and analysis," *Int. J. Solids Struct.*, vol. 40, no. 9, pp. 2147–2170, 2003.
- [32] Y. Murray, Manual for LS-DYNA wood material. Model 143, Report no. FHWA-HRT-04-097; US department of transportation, McLean, VA 22101-2296, USA, 2007.
- [33] J. P. Susainathan, "Development and characterization of wood based eco-structure," PhD University of Toulouse, 2017.
- [34] L. Mezeix, S. Dols, C. Bouvet, B. Castanié, J. P. Giavarini, and N. Hongkarnjanakul, "Experimental analysis of impact and post-impact behaviour of inserts in carbon sandwich structures," *J. Sandwich Struct. Mater.*, 2017. <http://dx.doi.org/10.1177/1099636216687582>.
- [35] L. Deka, and U. Vaidya, "LS-DYNA® impact simulation of composite sandwich structures with balsa wood core," 10th International LS-DYNA Users Conference, Detroit, 2008.
- [36] Forest Products Laboratory, Wood handbook—Wood as an engineering material. Madison, WI: Forest Products Lab. 2010.
- [37] A. Da Silva, and S. Kyriakides, "A compressive response and failure of balsa wood," *Int. J. Solids Struct.*, vol. 44, no. 25–26, pp. 8685–8717, 2007.
- [38] T. Maillot, V. Lapoujade, E. Gripon, B. Toson, N. Bardon, and J. J. Pesque, "Comparative study of material laws available in LS-DYNA® to improve the modeling of balsa wood," 13th International LS-DYNA Users Conference, Michigan, 2014.
- [39] A. M. Otkur, "Impact modeling and failure modes of composite plywood," Master thesis, Texas Tech University, 2010. <http://hdl.handle.net/2346/ETD-TTU-2010-12-1099>.
- [40] M. Ilyas, "Damage modeling of carbon epoxy laminated composites submitted to impact loading," Doctoral thesis, Université de Toulouse, France.
- [41] C. Bouvet, S. Rivallant, and J. J. Barrau, "Low velocity impact modeling in composite laminates capturing permanent indentation," *Compos. Sci. Technol.*, vol. 72, no. 16, pp. 1977–1988, 2012.